TPM Vol. 32, No. S3, 2025
ISSN: 1972-6325
https://www.tpmap.org/

Open Access

EXPERIMENTAL STUDY IN FLOW BOARD AND CFD OF VARIATIONS AND PRESSURES IN V SECTIONS TO ANALYZE THE DISSIPATION EFFECT

CASTILLO-PÉREZ SANTIAGO ALONSO[A], FERNANDEZ-AQUINO ISAAC JAREDH[B], CARMONA-ARTEAGA ABEL, MAGISTER SCIENTIAE EN RECURSOS HÍDRICOS[C]
[A,B,C]UNIVERSIDAD PRIVADA DEL NORTE, PERÚ
EMAILS; N00165706@upn.pe[A], N00228893@upn.pe[B], abel.carmona@upn.edu.pe[C]

ABSTRACT: In this study, the different variations of the velocities and pressures in V-sections are analyzed. These sections can be used in various structural designs. Using engineering software, the main objective is to understand the fluid variations and the energy dissipation due to the geometric sections designed and used in situations where energy dissipation is a critical factor, such as in pipeline systems, as well as in the design of structures that must resist the forces of a fluid, in addition to providing information for the design and optimization of systems that can help engineers make better decisions about the design of components that improve efficiency and safety.
Design and simulation software remains an important tool for the analysis of the effect in different flow configurations, giving detailed results about the velocities and pressures of different points of the designed sections, combining physical experiments and numerical simulations to investigate in detail the behavior of a fluid, since the results obtained are of great interest to engineers and scientists working in various areas, such as fluid mechanics.
Keywords: *Autodesk CFD, Dissipation, flows, Huaicos, laminar, turbulent.*

1. INTRODUCTION

Every year during the rainy season, landslides (also known as alluviums, avalanches and landslides) cause rapid-impact disasters, resulting in destroyed homes, affected families, devastated farmland, interrupted communication lines, paralysis of economic activities and other consequences in Lima. In addition, slow-impact disasters occur throughout the rural area consisting of the gradual degradation of the soil due to the erosive force of water. [1]
Over the years on the coast of Peru there have been climatic variations due to various factors, which have caused floods, landslides and even human losses.
Fig.1 shows how climatic factors on the coast of the country generated an increase in river flows which caused landslides and in certain sections of the city blocking access.

2. IMPORTANCE OF THE STUDY

The importance of the study is focused on determining the areas where the greatest pressure variations occur, which is fundamental to evaluating drag, erosion, and other flow energy dissipation phenomena affecting the V-shaped structures.

2.1 RESEARCH OBJECTIVE

In view of the above problems, the objective of this study is to graphically analyze the velocities and pressures exerted on the designed structures, experimentally and using CFD software, under laminar and turbulent conditions, in order to have a real-time and scaled perspective of the possible solutions and mitigation measures for possible natural disasters.

2.2 THEORETICAL FRAMEWORK

A. Energy Equation

This is the form of the energy equation that will be used most often in this book. As with Bernoulli's equation, each term in the equation represents an amount of energy per unit weight of fluid flowing in the system. [3]

$$\frac{V_1^2}{2g}+\frac{P_1}{\gamma}+Z_1=\frac{V_2^2}{2g}+\frac{P_2}{\gamma}+Z_2+H_t \quad (1)$$

B. Reynolds Number

The Reynolds number represents the effect of the viscosity of the fluid in relation to its inertia. Laminar flow occurs when NR< 500. The range from 500 to 2300 is the transitional range. In general, turbulent flow occurs when NR >2300. [4]

$$\mathrm{Re} = \frac{Dv\rho}{\mu} \quad (2)$$

C. Drag Force

The force exerted by a fluid on a body in the direction of flow is called drag. Drag can be measured directly by simply attaching the body immersed in a fluid flow to a calibrated spring and measuring the displacement in the direction of flow. [5]

$$F_D = Arrastre = C_D(\frac{\rho V^2}{2})A \quad (3)$$

D. Flow Rate

The term flow rate means: the volume of water that passes through a surface in a given time. A flow rate is calculated using the following formula: Q=V/t, where Q (flow rate), V (volume), and t (time). Usually, volume is measured in liters and time is measured in seconds. [6]

$$Q = \frac{V}{T} \quad (4)$$

E. Navier-Stokes

The density of the fluid is large enough to approximate a continuous medium, so that any infinitesimal portion of the fluid contains a sufficient number of particles to define a velocity and even an average kinetic energy in the infinitesimal element. In fluid mechanics, variables and properties averaged over an infinitesimal volume are defined by considering them as properties at each point of the fluid. [7]

$$\rho\frac{DV}{Dt} = -\nabla P + \rho g + \mu\nabla^2 v \quad (5)$$

F. Bernoulli's equation

Bernoulli's principle tells us that the equation is used to represent the equation of conservation of energy, speaking of a horizontal flow where the points of higher viscosity will have less pressure than those of lower velocity. [8]

$$\frac{\rho_1}{\rho g} + \frac{V_1^2}{2g} + Z_1 = \frac{\rho_2}{\rho g} + \frac{V_2^2}{2g} + Z_2 \quad (6)$$

G. Von Karman effect

The Von Karman effect is referred to as the Von Karman effect for rotating, confined flows with very high Reynolds numbers in relatively small volumes. As the flow approaches the front surface of the detaching element, it splits into two streams. [2]

The fluid close to the body has a lower velocity compared to the main flow velocity. This velocity difference results in the formation of shear layers, which eventually break into vortices alternately on both sides of the detachment element. The vortex wake is called Karman Street, after Theodor Von Karman, who discovered and characterized the phenomenon. [9]

H. Stagnation point

A stagnation point is defined as a point in the flow field where the velocity is exactly zero and where the fluid impinges squarely on either a projected area or a profile. [10]

I. Autodesk AutoCAD

In AutoCAD software is used for. Draw and annotate 2D geometry and 3D models with solids, surfaces and mesh objects, automate tasks, and create a customized workspace to maximize productivity with add-on applications. [11]

J. Autodesk Inventor

Inventor® 3D CAD software, offers professional tools for mechanical design, documentation development and product simulation. Efficient combination of parametric, direct, free-form and rule-based design functions. Integrated tools for structural, tube and pipe design.[12].

K. Autodesk CFD

Autodesk® CFD (Computational Fluid Dynamics) software creates computational fluid dynamics simulations to intelligently predict how liquids and gases will behave and analyze heat transfer and fluid flow design. [13]

L. Laminar Case Method

Some flows are smooth and orderly while others are considered chaotic. The intensely ordered motion of a fluid, characterized by undisturbed layers is known as laminar. The word laminar comes from the movement of particles together in the fluid, in “sheets.” [14]

M. Method for turbulent case

SST K-Omega SAS: The Scale-Adaptive Simulation (SAS) concept is based on the introduction of the Von Karman length scale into the turbulence scaling equation. The information provided by the Von Karman length scale allows SAS models to dynamically fit structures solved in a URANS simulation. [15]

2.3 METHODOLOGY

A. Dessing and Modeling of the Structure System

In Figure 1, the structures are defined through the basic design in AutoCAD, using Autodesk Inventor to assign the "PATCH" command, which defines the flow domain and modifies its performance to proceed to its simulation in Autodesk CFD.

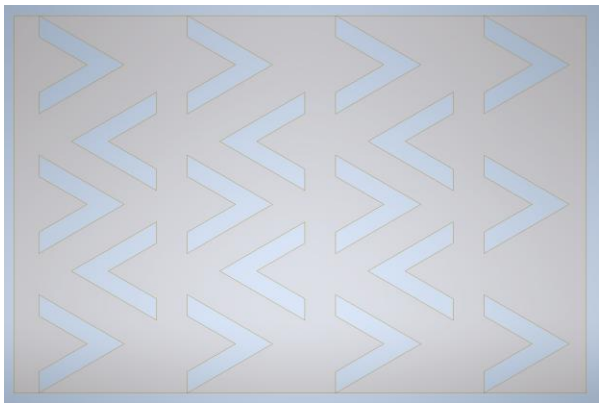

Fig.1 Modeled in AutoCAD passed to Inventor CFD.

B. Steps for its physical simulation

Using the AutoCAD design for the extraction of measurements, a formwork was built in which we poured a mixture of water and gypsum, after drying it was sanded and waterproofed to obtain waterproof solids in real scale to be simulated in the flow table.

In Fig.2 we can see the casting and setting of the solids made with plaster, some of them already stripped and ready to be sanded and waterproofed.

Fig.2 Solid physically.

C. Steps for CFD Simulation

In Figure 3 we can observe a flowchart that shows the process to be followed for the final development of the structural system for its simulation, taking it through different software, starting from AutoCAD and finally arriving at Autodesk CDF.

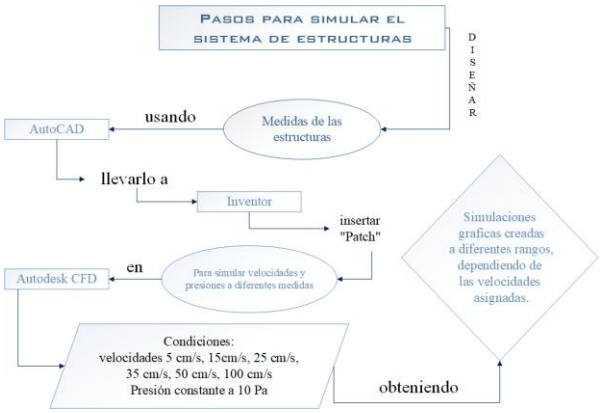

Fig.3 Flowchart.

2.4 RESULTS

A. Reynolds Number Calculation

In Table 1 we have the data used to calculate the Reynolds number and qualify the flow according to its type.

General Data			
Temperature	ρ	μ	I. diameter
°C	Kg/m3	Pas	M
20	998.57778	1.02E-03	0.00995049

Table 2 calculates the surface area of the laminar flow bench using the width and height in meters.

Surface area		
Width (m)	Height (m)	Area (m2)
0.5	0.005	0.0025

In Table 3, we will use the velocities in m/s and the area in m2 to calculate the flow rates.

Flow Calculation			
Vel. (cm/s)	Vel. (m/s)	Area (m2)	Flow rate (m3/s)
5	0.05	0.0025	0.000125
15	0.15	0.0025	0.000375
25	0.25	0.0025	0.000625
35	0.35	0.0025	0.000857
50	0.50	0.0025	0.00125
100	1.00	0.0025	0.0025

Table 4 to determine the Reynolds number using the velocity, density, dynamic viscosity and internal diameter of the pipe. This is used to determine the resulting flow type and qualify it as Laminar (L.) or Turbulent (T.).

Determine Reynolds number					
V. (m/s)	ρ (Kg/m3)	μ (Pas)	I D (m)	Reynolds	

0.05	998.57778	0.00120	0.0099525	487.0636	L
0.15	998.57778	0.00120	0.0099525	1461.1908	L
0.25	998.57778	0.00120	0.0099525	2435.3180	T
0.35	998.57778	0.00120	0.0099525	3409.4452	T
0.50	998.57778	0.00120	0.0099525	4870.6359	T
1.00	998.57778	0.00120	0.0099525	9471.2719	T

After knowing the velocities, pressures, and the correct classification of the flow type, we proceed to input the data into the CFD software for simulation. For this study, we will use the same inlet and outlet pressure in all simulations to obtain a representative and approximate graph of the flow behavior.

B. Simulation of velocities and pressures at 5cm/s

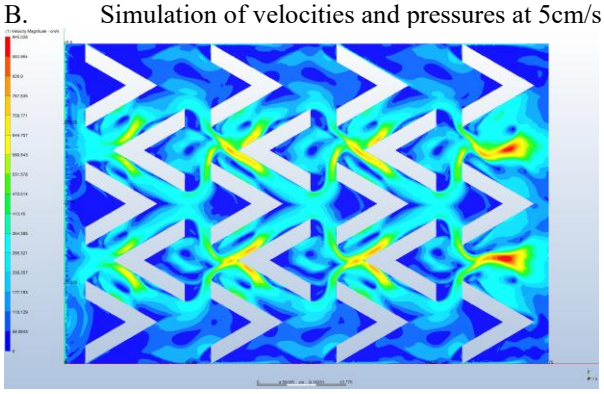

Fig.4 Simulation of velocity at 5cm/s.

Fig.4 shows the observation of the velocity at 5cm/s, in the central part of the system of structures, the maximum velocities are found in a range from 236.26cm/s to 945.03cm/s, specifically at the tips of the solids in the central zone.

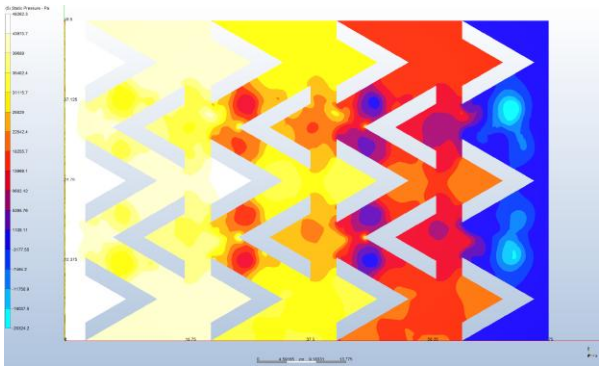

Fig.5 Simulation of pressure at 5cm/s.

Fig. 5 shows that the highest pressure is 48262.3Pa and is found where the fluid enters. The minimum values are -20324.2Pa, being negative when leaving the whole system of structures.

C. Simulation of velocities and pressures at 15cm/s

TPM Vol. 32, No. S3, 2025
ISSN: 1972-6325
https://www.tpmap.org/

Open Access

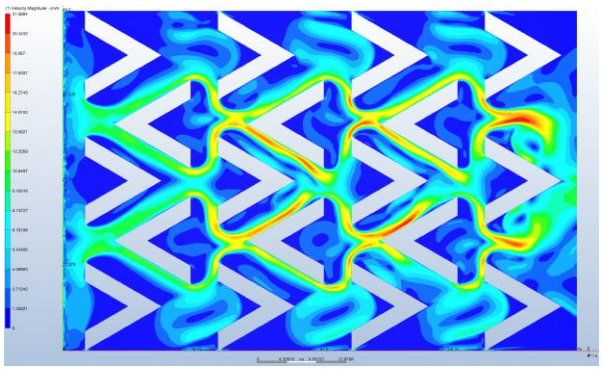

Fig.6 Simulation of velocity at 15cm/s.

Fig.6 shows the simulation at a velocity of 15cm/s. In the central part of the structure system, the maximum velocities are found in a range from 2.71cm/s to 21.70cm/s, especially in the central zone of the structures.

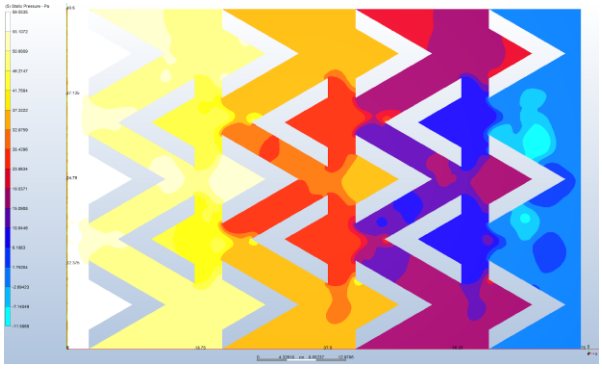

Fig.7 Simulation of pressure at 15cm/s.

In Fig.7 a higher pressure 59.55Pa is observed where the fluid enters. On the other hand, the minimum values are -11.59Pa which are negative due to the force it loses while passing through the system of structures at the moment of exit.

D. Simulation of Velocities and Pressures at 25cm/s

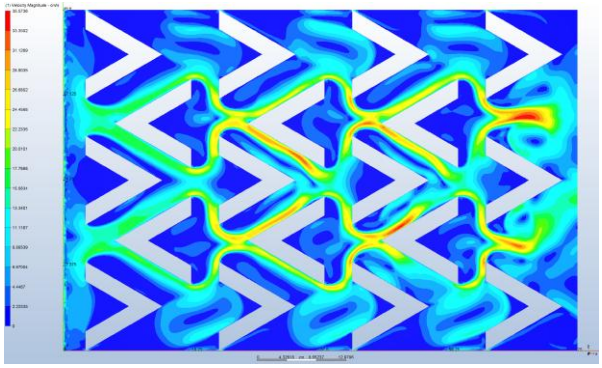

Fig.8 Simulation of velocity at 25cm/s.

Fig.8, in the 25cm/s simulation, we can observe the upper and lower parts as vorticity is generated due to the velocity with which the fluid enters and impacts with the first rows of the structure system.

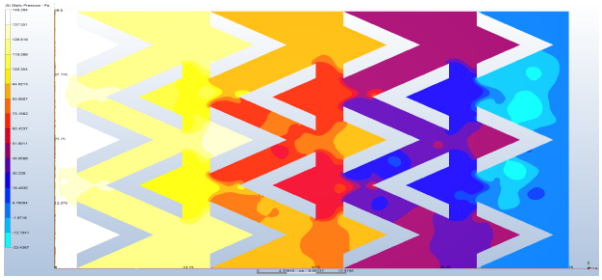

Fig.9 Simulation of pressure at 25cm/s.

Fig.9 shows an increase in pressure loss compared to Fig.8 when the fluid reaches a pressure of -23.44Pa.

E. Simulation of velocities and pressures at 35cm/s.

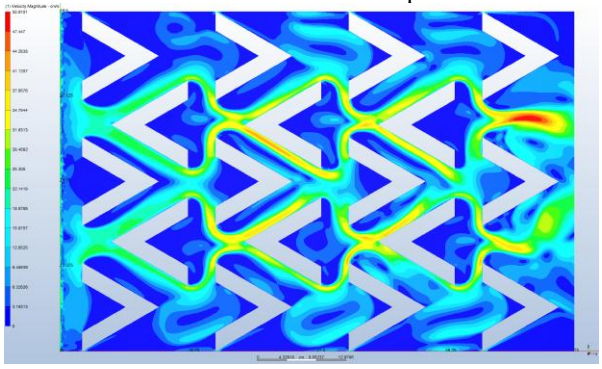

Fig.10 Simulation of velocity at 35cm/s.

In Figure 10, in the middle right zone, it can be seen that the fluid exits the system at a higher velocity than the inlet velocity and reaches critical levels of 50.61 cm/s.

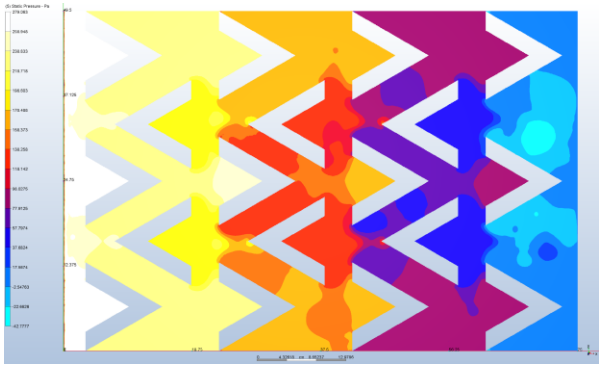

Fig.11 Simulation of pressure at 35cm/s.

Figure 11 shows that the highest pressure is 279.06Pa and is found on the left side where the fluid enters. The minimum values are -42.78Pa, being negative when leaving the whole system of structures.

F. Simulation of velocities and pressures at 50 cm/s.

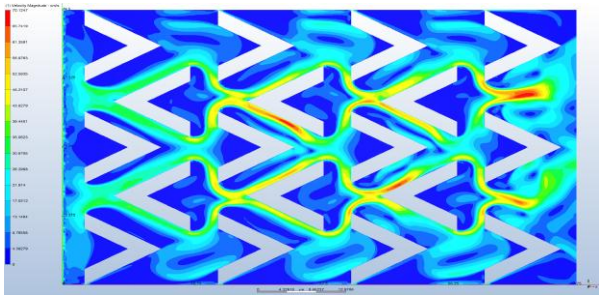

Fig.12 Simulation of velocity at 50cm/s.

In Fig.12 the simulation of the velocity at 50 cm/s is observed, in the central part of the system of structures the maximum velocities are found in a range from 236.26 cm/s to 945.03 cm/s, specifically at the tips of the solids in the central zone.

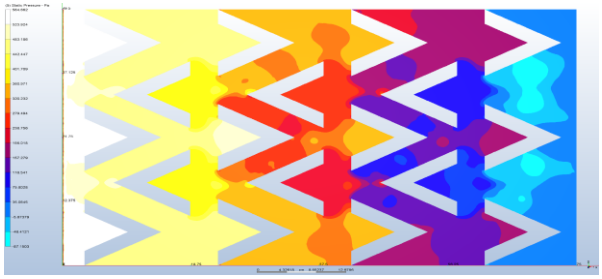

Fig.13 Simulation of pressure at 50cm/s.

Fig.13 shows that the highest pressure is 564.66Pa and is found in the zone where the fluid enters. The minimum values are -87.15Pa and are negative at the exit of the whole system of structures.

TPM Vol. 32, No. S3, 2025
ISSN: 1972-6325
https://www.tpmap.org/

Open Access

G. Simulation of Velocities and Pressures at 100cm/s.

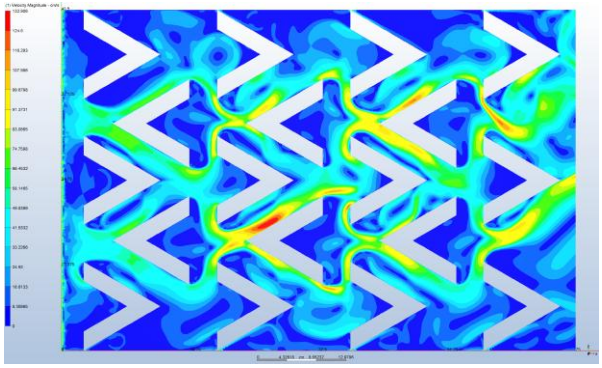

Fig.14 Simulation of velocity at 100cm/s.

In Fig.14, the simulation of the velocity at 100 cm/s, from the third column to the last column, the maximum velocities in the range of 16.61 cm/s to 132.91 cm/s.

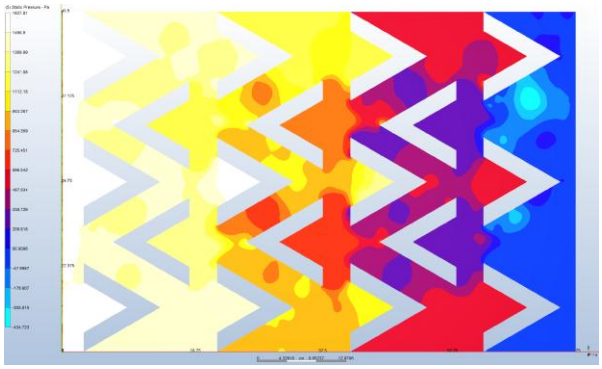

Fig.15 Simulation of pressure at 100cm/s

In Fig.15 it was possible to appreciate that at the moment of leaving the system of structures the fluid has not so low pressures in comparison to the previous simulations, with a pressure of -176.91Pa being thus the lowest pressures of all in spite of having a higher entrance velocity.

At the end of the simulations in the software used, we proceeded with the study of the V-shaped structural sections on the flow table, either laminar or turbulent. It was determined at a height of 12 cm or 0.12 m with different time variations for each centimeter to obtain a laminar or turbulent flow.

H. Laminar

As can be seen in Figure 16, the flow with ink, when colliding with the structures, we observe how the drag or also called turbulent wake is generated due to the negative pressures.

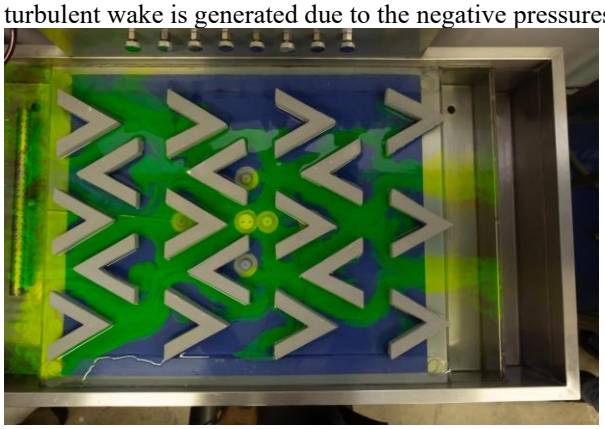

Fig.16 Simulation on the flow table for laminar case.

I. Turbulent

In the case of turbulent flow, it is shown that when the fluid hits the structures through the separation points, the change in flow direction creates vortices that cause friction between the water molecules, resulting in energy loss as shown in Figure 17.

Fig.17 Simulation on the flow table for laminar case.

Figure 18 shows the analysis during the experimental realization, the process carried out and the observations made during the execution of the project on the flow table located in the Hydraulics Laboratory of the Universidad Privada del Norte, located in the district of Breña.

Fig.18 Evidence of experimental development.

J. Reynolds Number Calculation by Experimental Method

In Table 5 we have the data used to calculate the Reynolds number and qualify the flow according to its type.

General Data			
Temperature	ρ	μ	I. diameter
°C	Kg/m3	Pas	M
19.2	998.716444	1.02E-03	0.002475

In Table 6 we will use the width and height in meters for the calculation of the surface area of the laminar flow bench.

Surface area		
Width (m)	Height (m)	Area (m2)
0.5	0.005	0.0025

In Table 7 we have the calculation of Q which was used for the Reynolds number calculation, the result is a laminar flow of 310,108.

Determine Reynolds number laminar case				
cumulative	**cumulative time (s)**	**part-time**	**h/t**	**Q**

difference (m)				
0.01	4.57	4.57	0	0
0.02	15.30	0.0012	0.000932	0.00035
0.03	27.08	0.0012	0.000849	0.00032
0.04	38.68	0.0012	0.000862	0.00032
0.05	51.56	0.0012	0.000776	0.00029
0.06	66.07	0.0012	0.000689	0.00026
0.07	78.07	0.0012	0.000833	0.00031
0.08	89.71	0.0012	0.000859	0.00032
0.09	100.94	0.0012	0.000890	0.00033
0.10	112.96	0.0012	0.000832	0.00031
0.11	124.33	0.0012	0.000880	0.00033
0.12	135.34	0.0012	0.000908	0.00034

In Table 8 we have the calculation of Q which was used for the Reynolds number calculation, the result is a turbulent flow of 3346.168.

Determine Reynolds number turbulent case				
cumulative difference (m)	**cumulative time (s)**	**part-time**	**cumulative difference (m)**	**Q**
0.01	2.61	4.57	0	0
0.02	4.77	0.00120	0.0099525	1461.1908
0.03	9.21	0.00120	0.0099525	2435.3180
0.04	13.30	0.00120	0.0099525	3409.4452
0.05	18.65	0.00120	0.0099525	4870.6359
0.06	23.74	0.00120	0.0099525	9471.2719
0.07	27.76	0.00120	0.0099525	1461.1908
0.08	31.73	0.00120	0.0099525	2435.3180
0.09	36.13	0.00120	0.0099525	3409.4452
0.10	41.09	0.00120	0.0099525	4870.6359
0.11	44.60	0.00120	0.0099525	9471.2719
0.12	49.78	0.00120	0.0099525	4870.6359

3. CONCLUSIONS

The experimental study on flow table and CFD of variations and pressures in V-sections to analyze the dissipation effect provides valuable insight into the flow behavior and pressure distribution in this type of channels. The information obtained is useful for the design and analysis of hydraulic systems with V-sections, taking into account the effect of energy dissipation.

Proceeding to CFD simulation allowed us to obtain in more detail the distribution of pressures exerted on the V-shaped structures, such as high and low pressure zones. This was important because between the simulation in the software and the experimental simulation in the flow table, it showed a great similarity, which would be valid in the methodology used.

REFERENCES

[1] Diario El Comercio “Emergencia en Punta Hermosa: alertan huaico de grandes proporciones” https://larepublica.pe/sociedad/2023/03/18/huaico-en-punta-hermosa-municipalidad-alerta-deslizamiento-de-grandes-proporciones-en-playa-norte-y-central-348192

[2] R. Mott and J. Untener. “Mecánica de fluidos (7na ed.)”, editorial Addison Wesley (2015), pp 159, 375, 404, 405, 406, 434, 488.
[3] Y. Cengel and J. Cimbala. “Mecánica de fluidos: fundamentos y aplicaciones (2da ed.)”, editorial McgrawHill (2015), pp133, 586, 593.
[4] F.R. Menter ResearchGate, 2006. “A scale-adaptive simulation model using two-equation models.” https://www.researchgate.net/publication/281053423_A_scale-adaptive_simulation_model_using_two-equation_models
[5] Productos de autodesk. https://www.autodesk.es/
[6] Libro Mecánica de fluidos. Apuntes de Agustin Martin Domingo, pp37, 40, 42, 53.
[7] Campo Correa, Jesús Alberto; Stephanie Díaz Umaña; Humberto Ávila Rangel; German Daniel Rivillas-Ospina. “Estimación del potencial de disipación de energía del oleaje de estructuras sumergidas y flotantes.” doi.org: 10.14483/22487638.13387
[8] Zhang, Jian; Lou, Yibing. Frontiers in Marine Science; Lausanne (Apr 3, 2024). “Study of wave-current coupling on offshore flexible photovoltaic foundation columns.” doi.org: 10.3389/fmars.2024.1387353
[9] Zainul Faizien Haza. IOP Conference Series. Materials Science and Engineering; Bristol Tomo 316, N.º 1, (Mar 2018). “The drag forces exerted by lahar flows on a cylindrical pier: case study of post Mount Merapi eruptions.” doi.org: 10.1088/1757-899X/316/1/012041
[10] Shi, John Z. Atmosphere; Basel Tomo 15, N.º 4, (2024): 494. “Some Early Studies of Isotropic Turbulence: A Review.” doi.org: 10.3390/atmos15040494.
[11] Blagojević, Marko; Hočevar, Marko; Bizjan, Benjamin; Drešar, Primož; Sabina Kolbl Repinc ; et al.. Water; Basel Tomo 16, N.º 12, (2024): “Three-Dimensional Numerical Simulation of a Two-Phase Supercritical Open Channel Junction Flow.” doi.org: 10.3390/w16121757
[12] Zhang, Shuai; Law, Adrian Wing-Keung. Water; Basel Tomo 16, N.º 2, (2024) “Performance of Reynolds Averaged Navier–Stokes and Large Eddy Simulation Models in Simulating Flows in a Crossflow Ultraviolet Reactor: An Experimental Evaluation” doi.org: 10.3390/w16020271
[13] Liu, Jiawei; Lu, Junliang; Liang, Zejun. Water; Basel TTomo 16, N.º 14, (2024): 1940. “Computational Simulation of Monopile Scour under Tidal Flow Considering Suspended Energy Dissipation” doi.org: 10.3390/w16141940
[14] Zadeh, Seyed Mehdi Naghib; Heidarnejad, Mohammad; Masjedi, Alireza; Kamanbedast, Amirabbas; Bordbar, Amin “Comparación de la disipación de energía en aguas abajo de aliviaderos escalonados y desconcertados de vertederos de tecla de piano.” doi.org: 10.24850/j-tyca-2020-04-07
[15] Liu, Weiqin; Liu, Tao; Hu, Qi; Wang, Mingzhen; Song, Xuemin; Chen, Hao “A High-Efficiency Theorical Model of Von Karman–Generalized Wagner Model–Modified Logvinovich Model for Solving Water-Impacting Problem of Wedge.” doi.org: 10.3390/jmse12071125
[16] M. Yglesias, A Valdés, S. Hartinger, K.Takahashi, G. Salvatierra, R. Velarde, A. Contreras, R. Contreras, V. Paz, J. Bazo, A. Lescano, “Reflections on the impact and response to the Peruvian 2017 Coastal El Niño event: Looking to the past to prepare for the future.” doi.org: 10.1371/journal.pone.0290767
[17] Juan Carlos Espinosa García, Juan Carlos Mera Tobar, “Análisis experimental de disipación de energía, distribución de presiones y resistencia al flujo de una rápida con fondo escalonado con relación altura (h) longitud de grada (I) de h/l=0.10.” http://bibdigital.epn.edu.ec/handle/15000/520
[18] Juan Bedoya Cristancho, Santiago Cerón Vivas, “Modelación numérica de la socavación local en los estribos del puente sobre el río Sunuba según las características hidrodinámicas de la zona.” http://hdl.handle.net/10554/21400
[19] Francisco Briceño, Henry Sifuentes, “Estudio del comportamiento hidrodinámico del puente del rio Moche y evaluación frente a los efectos de erosión y socavación en los pilares, la libertad, Trujillo 2019.” https://hdl.handle.net/20.500.12759/5154
[20] J. Marañón Di Leo, M.V. Calandra, J.S. Delnero, “Change point algorithms applied to the detection of vortex structures in turbulent flows.” Doi.org: 10.1016/j.rimni.2016.04.009
[21] T. l. d. reservados, «Autodesk,» 2023. https://help.autodesk.com/view/SCDSE/2023/ENU/?guid=GUID0F5C4828-9F91-46B6-A16A-2578D72DCFCC.
[22] Quishpe Songor, Diego Javier, “Manual de prácticas virtuales de laboratorio, aplicando modelación numérica (CFD) para uso en las asignaturas de mecánica de fluidos e hidráulica aplicada.” http://dspace.ups.edu.ec/handle/123456789/20753
[23] Newton F. Ouedraogo, Ebenezer E. Essel, “Effects of Reynolds Number on the Wake Characteristics of a Notchback Ahmed Body.” doi.org: 10.1115/1.4065225
[24] Yannick Marschall; George Constantinescu; Robert M. Boes; David F. Vetsch, “On the Role of Free-Surface Treatment for Simulating Flow Past Submerged Obstacles.” doi.org: 10.3850/978-90-833476-1-5_iahr40wc-p0071-cd
[25] B. Matthew, H. Alejandra, L. Erika, L. Vicente, “Everything that Rises Must Converge: Huaicos, Communitas, and Humanitarian Exchange in Peru.” doi.org: 10.17730/1938-3525-79.3.